JOURNAL OF GUIDANCE, CONTROL, AND DYNAMICS
Vol. 18, No. 6, November–December 1995

Motion of a Rigid Body with an Attached Spring-Mass Damper

Anne E. Chinnery* and Christopher D. Hall†
U.S. Air Force Institute of Technology, Wright–Patterson Air Force Base, Ohio 45433

The stability of motion of a torque-free rigid body with a precession damper is investigated. The equations of motion are presented and nondimensionalized, and the well-known conditions for asymptotic stability of the major axis spin are stated. Attention is given to the cases where these conditions are not met. Results of numerical integration are used to identify three distinct types of motion, including solutions that are apparently limit cycles. Bifurcation diagrams are used to argue that the apparent limit cycles are actually slowly approaching an equilibrium. The bifurcation diagrams also identify regions where the jump phenomenon may occur. The Lyapunov–Schmidt reduction technique is used to obtain a simple analytical relationship between the system parameters that determines whether the jump phenomenon is possible.

Introduction

SPIN stabilization of satellites depends on the effective use of energy dissipation to damp out coning motions caused by perturbing torques. The major axis rule[1] is one well-known design criterion for spin stabilized satellites with unspecified energy dissipation, but this rule must be modified for specific damping mechanisms. For example, the major axis rule is not sufficient for stability of a satellite with a precession damper of the type studied here. The purpose of this paper is to present some new results on the stability of motion of such systems.

This problem has been studied by numerous authors. Cloutier[2] studied the related problem of nutation dampers on both spin and dual-spin stabilized spacecraft, and identified the possibility of coexisting stable equilibria. Schneider and Likins[3] prescribed the damper motion and used an approximate analysis to compare the effectiveness of precession and nutation dampers. Spin and dual-spin spacecraft were studied by Sarychev and Sazonov,[4] and they obtained criteria for stability of the steady spin, as well as for optimal damping of small cone angles. Cochran and Thompson[5] compared nutation and precession dampers and obtained an approximate analytical formula for energy dissipation rates. Month and Rand[6] used perturbation methods and computer algebra to determine stability conditions of a rigid body with an attached spring-mass oscillator with prescribed motion. Levi[7] identified multiple equilibria and nonsteady solutions for a system with the damper on a principal axis and the undeformed mass center fixed. Kane and Levinson[8] introduced a new dissipation mechanism for axisymmetric bodies and gave a lengthy list of references to previous work in this area. Chinnery[9] used a Lyapunov function analysis to obtain the same stability conditions as Sarychev and Sazonov.[4] Hughes[1] used this problem as a textbook example with a detailed linearized stability analysis.

In this paper we study the dynamics of a rigid body with a precession damper, using simulation, numerical continuation, and analytical bifurcation theory. We begin by stating the equations of motion as developed by Hughes,[1] which we nondimensionalize.[9] We then state the stability conditions[1,4,9] in terms of dimensionless parameters. We are primarily interested in what happens when these conditions are not met. Numerical simulation results are used to identify three distinct types of motion, including a persistent oscillation that appears to be a limit cycle. It is this apparent limit cycle that motivates our bifurcation analysis. Continuation methods[10,11] are used to develop bifurcation diagrams that indicate that the limit cycle is actually slowly moving toward an equilibrium. There are three different types of bifurcation diagrams, all of which exhibit multiple coexisting stable solutions and two of which permit the jump phenomenon. Separating the three types of bifurcation diagrams are two critical bifurcations: one a transcritical and one a degenerate pitchfork. The Lyapunov–Schmidt method[12,13] is used to obtain an analytical relationship between the system parameters defining the degenerate pitchfork.

Received May 27, 1994; presented as Paper 94-3715 at the AIAA/AAS Astrodynamics Conference, Scottsdale, AZ, Aug. 1–3, 1994; revision received Dec. 20, 1994; accepted for publication May 18, 1995. This paper is declared a work of the U.S. Government and is not subject to copyright protection in the United States.

*Graduate Student, Astronautical Engineering; currently Foreign Technology Analyst, National Air Intelligence Center.

†Assistant Professor of Aerospace and Systems Engineering. Senior Member AIAA.

Equations of Motion

The model we study is shown in Fig. 1, consisting of a rigid body $\mathcal{B}$, and a mass particle $\mathcal{P}$ that is constrained to move along a line $\boldsymbol{n}$ fixed in $\mathcal{B}$. For a precession damper, $\boldsymbol{n}$ is parallel to $\hat{\boldsymbol{e}}_2$, which is the nominal spin axis for the spacecraft. The reference axes $\hat{\boldsymbol{e}}_i$ are system principal axes when $\mathcal{P}$ is in its rest position ($\xi^* = 0$).

The dimensional equations of motion as derived by Hughes[1] are given next. The system linear and angular momentum are denoted by $\boldsymbol{p}^*$ and $\boldsymbol{h}^*$, respectively. (The superscript asterisk is used to denote dimensional quantities.) The linear momentum of the particle in the $\boldsymbol{n}$ direction is p_n^*, and the relative positive and velocity of the particle in the $\boldsymbol{n}$ direction are ξ^* and ζ^*. The angular velocity of the body frame is ω^*, and the velocity of the point $\boldsymbol{O}$ is $\boldsymbol{v}_o^*$. The position vector from $\boldsymbol{O}$ to $\mathcal{P}$ is $\boldsymbol{r}_p^* = \boldsymbol{b}^* + \xi^*\boldsymbol{n}$, where $\boldsymbol{b}^* = b^*\hat{\boldsymbol{e}}_1$. The mass of the particle is m_p^*, and the total mass is m^*. The first and second moments of inertia are $\boldsymbol{c}^* = m_p^*\xi^*\boldsymbol{n}$ and

$$\boldsymbol{J}^* = \begin{bmatrix} I_1^* + m_p^*\xi^{*2} & -m_p^*b^*\xi^* & 0 \\ -m_p^*b^*\xi^* & I_2^* & 0 \\ 0 & 0 & I_3^* + m_p^*\xi^{*2} \end{bmatrix} \tag{1}$$

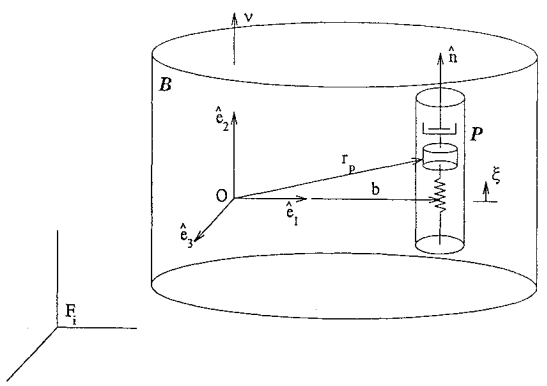

Fig. 1 System model.

The spring has stiffness k^*, and the dashpot damper has damping coefficient c^*. In terms of these variables and parameters, the equations describing torque- and force-free motion are

$$\boldsymbol{p}^* = m^*\boldsymbol{v}_o^* - \boldsymbol{c}^{*\times}\boldsymbol{\omega}^* + m_p^*\zeta^*\boldsymbol{n} \tag{2}$$

$$\boldsymbol{h}^* = \boldsymbol{c}^{*\times}\boldsymbol{v}_o^* + \boldsymbol{J}^*\boldsymbol{\omega}^* + m_p^*\zeta^*\boldsymbol{b}^{*\times}\boldsymbol{n} \tag{3}$$

$$p_n^* = m_p^*\left(\boldsymbol{n}^T\boldsymbol{v}_o^* - \boldsymbol{n}^T\boldsymbol{b}^{*\times}\boldsymbol{\omega}^* + \zeta^*\right) \tag{4}$$

$$\dot{\boldsymbol{p}}^* = -\boldsymbol{\omega}^{*\times}\boldsymbol{p}^* \tag{5}$$

$$\dot{\boldsymbol{h}}^* = -\boldsymbol{\omega}^{*\times}\boldsymbol{h}^* - \boldsymbol{v}_o^{*\times}\boldsymbol{p}^* \tag{6}$$

$$\dot{p}_n^* = m_p^*\boldsymbol{\omega}^{*T}\boldsymbol{n}^\times\left(\boldsymbol{v}_o^* - \boldsymbol{r}_p^{*\times}\boldsymbol{\omega}^*\right) - c^*\zeta^* - k^*\xi^* \tag{7}$$

$$\dot{\xi}^* = \zeta^* \tag{8}$$

The superscript $\times$ denotes the skew-symmetric matrix form of a vector.[1]

To nondimensionalize the equations, we first note that since there are no external torques, the angular momentum vector has constant magnitude; i.e., $\|\boldsymbol{h}^*\| = h^*$. We now define dimensionless variables and parameters as follows:

$$\begin{aligned}
\boldsymbol{p}^* &= \left(h^*m^*b^*/I_2^*\right)\boldsymbol{p} \qquad \boldsymbol{v}_o^* = \left(h^*b^*/I_2^*\right)\boldsymbol{v}_o \qquad t^* = \left(I_2^*/h^*\right)t \\
\boldsymbol{h}^* &= h^*\boldsymbol{h} \qquad \boldsymbol{\omega}^* = \left(h^*/I_2^*\right)\boldsymbol{\omega} \qquad \boldsymbol{b}^* = b^*\boldsymbol{b} \\
p_n^* &= \left(h^*m^*b^*/I_2^*\right)p_n \qquad \zeta^* = \left(h^*b^*/I_2^*\right)z \qquad \boldsymbol{J}^* = I_2^*\boldsymbol{J} \\
\xi^* &= b^*x
\end{aligned} \tag{9}$$

and introduce four dimensionless parameters:

$$\varepsilon = m_p^*/m^* \tag{10}$$

$$b = m^*b^{*2}/I_2^* \tag{11}$$

$$c = c^*I_2^*/(m^*h^*) \tag{12}$$

$$k = k^*I_2^{*2}/(m^*h^{*2}) \tag{13}$$

The parameter ε represents the mass fraction of the damper relative to the total system mass; we also use $\varepsilon' \triangleq 1 - \varepsilon$. The parameters c and k represent the damping coefficient and spring constant, respectively, and b characterizes the distance of the precession damper from the origin. The parameter b is closely related to the system radius of gyration about the $\hat{\boldsymbol{e}}_2$ axis, k_g^*, since

$$I_2^* = m^*k_g^{*2} \tag{14}$$

The value $b = 1$ puts the precession damper at the radius of gyration. The dimensionless form of the inertia matrix is

$$\boldsymbol{J} = \begin{bmatrix} I_1 + \varepsilon bx^2 & -\varepsilon bx & 0 \\ -\varepsilon bx & 1 & 0 \\ 0 & 0 & I_3 + \varepsilon bx^2 \end{bmatrix} \tag{15}$$

The nondimensional equations are

$$\boldsymbol{p} = \boldsymbol{v}_o - (1/b)\boldsymbol{c}^\times\boldsymbol{\omega} + \varepsilon z\boldsymbol{n} \tag{16}$$

$$\boldsymbol{h} = \boldsymbol{c}^\times\boldsymbol{v}_o + \boldsymbol{J}\boldsymbol{\omega} + \varepsilon bz\boldsymbol{b}^\times\boldsymbol{n} \tag{17}$$

$$p_n = \varepsilon\left(\boldsymbol{n}^T\boldsymbol{v}_o - \boldsymbol{n}^T\boldsymbol{b}^\times\boldsymbol{\omega} + z\right) \tag{18}$$

$$\dot{\boldsymbol{p}} = -\boldsymbol{\omega}^\times\boldsymbol{p} \tag{19}$$

$$\dot{\boldsymbol{h}} = -\boldsymbol{\omega}^\times\boldsymbol{h} - b\boldsymbol{v}_o^\times\boldsymbol{p} \tag{20}$$

$$\dot{p}_n = \varepsilon\boldsymbol{\omega}^T\boldsymbol{n}^\times\left(\boldsymbol{v}_o - \boldsymbol{r}_p^\times\boldsymbol{\omega}\right) - cz - kx \tag{21}$$

$$\dot{x} = z \tag{22}$$

Since there are no external forces linear momentum is conserved, and we assume without loss of generality that $\boldsymbol{p} = \boldsymbol{0}$. We then eliminate $\boldsymbol{v}_o$ and $\boldsymbol{\omega}$ from Eqs. (20–22), obtaining a fifth-order system,

$$\dot{\boldsymbol{h}} = \boldsymbol{h}^\times\boldsymbol{K}^{-1}\boldsymbol{L} \tag{23}$$

$$\dot{p}_n = -\varepsilon\boldsymbol{L}^T\boldsymbol{K}^{-1}\boldsymbol{n}^\times[(\varepsilon' x\boldsymbol{n} + \boldsymbol{b})^\times\boldsymbol{K}^{-1}\boldsymbol{L} + \varepsilon\dot{x}\boldsymbol{n}] - c\dot{x} - kx \tag{24}$$

$$\dot{x} = \frac{p_n/\varepsilon + \boldsymbol{n}^T\boldsymbol{b}^\times\boldsymbol{K}^{-1}\boldsymbol{h}}{\varepsilon' + \varepsilon b\boldsymbol{n}^T\boldsymbol{b}^\times\boldsymbol{K}^{-1}\boldsymbol{b}^\times\boldsymbol{n}} \tag{25}$$

where

$$\boldsymbol{L} = \boldsymbol{h} - \varepsilon b\dot{x}\boldsymbol{b}^\times\boldsymbol{n} \tag{26}$$

$$\boldsymbol{K}^{-1} = \begin{bmatrix} 1/D_1 & \varepsilon bx/D_1 & 0 \\ \varepsilon bx/D_1 & D_2/D_1 & 0 \\ 0 & 0 & 1/D_3 \end{bmatrix} \tag{27}$$

$$D_1 = I_1 + \varepsilon b(\varepsilon' - \varepsilon b)x^2 \tag{28}$$

$$D_2 = I_1 + \varepsilon\varepsilon' bx^2 \tag{29}$$

$$D_3 = I_3 + \varepsilon\varepsilon' bx^2 \tag{30}$$

These equations are used in the numerical studies reported in this paper.

Stability Criteria

The desired motion corresponds to a steady spin about the $\hat{\boldsymbol{e}}_2$ axis, $\boldsymbol{h} = (0, 1, 0)$, $x = \dot{x} = 0$, which is easily shown to satisfy the equilibrium conditions $\dot{\boldsymbol{h}} = \boldsymbol{0}$, $\dot{p}_n = \dot{x} = 0$. For a rigid body this is a marginally stable motion if $\hat{\boldsymbol{e}}_2$ is the major or minor axis. For a quasirigid body with very slow energy dissipation, the nominal spin is asymptotically stable only if $\hat{\boldsymbol{e}}_2$ is the major axis and unstable otherwise. For the finite energy dissipation provided by the precession damper, the result is not as simple. Sarychev and Sazonov[4] and Hughes[1] used linearization and the Routh–Hurwitz criteria to obtain conditions for stability of the steady spin. Chinnery[9] derived the same conditions using a Lyapunov function consisting of the rotational kinetic energy plus spring potential energy constrained by the constant magnitude of the angular momentum vector. In terms of our dimensionless parameters, the stability criteria are

$$I_2 > I_3 \tag{31}$$

$$I_2 > I_1 + \varepsilon^2 b/k \tag{32}$$

Note that it is not sufficient that the body be oblate. Also, note that in our nondimensionalization, we have $I_2 = 1$, so the second condition may be written as

$$k > \varepsilon^2 b/(1 - I_1) \tag{33}$$

As we subsequently demonstrate, this relationship between the parameters corresponds to a pitchfork bifurcation. We assume throughout that the major axis conditions are met; i.e., $I_2 > I_1$, and $I_2 > I_3$.

Numerical Integration Results

As already noted, we are particularly interested in the system response when the stability criteria are not satisfied. We would like to answer the question: What other limiting motions are possible as $t \to \infty$?

In this section, we present simulation results for stable and unstable cases, obtained by numerical integration of Eqs. (23–25). In Figs. 2–4 we plot the transverse angular momenta h_3 vs h_1 for an asymmetric spacecraft with $I_1 = 0.6664$, $I_3 = 0.5$, and $\varepsilon = 0.1$. In all three plots, the initial conditions are $\boldsymbol{h} = (0.00999, 0.999, 0.00999)$, $x = p_n = 0$. Note that the scales of the three plots are different.

The first case (Fig. 2) is the stable case; i.e., Eqs. (31) and (32) are satisfied. As expected, the small initial cone angle is diminished by the energy dissipation. In the second case (Fig. 3) the solution

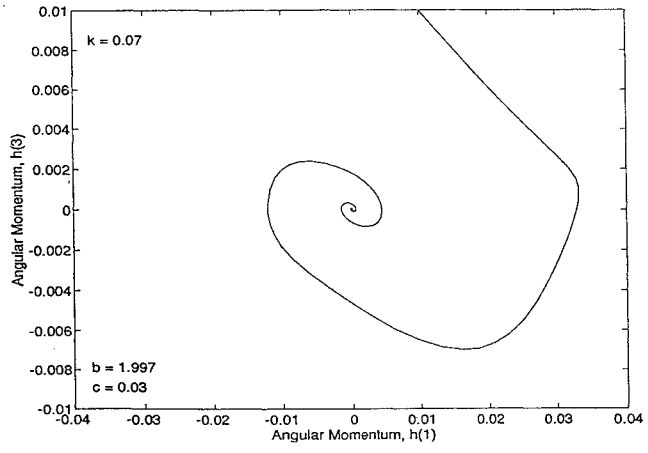

Fig. 2 Stable nominal motion: trajectory spirals into origin; Eq. (33) is satisfied.

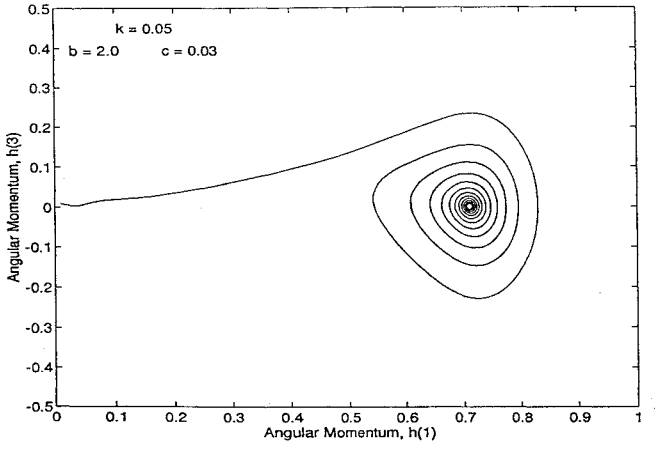

Fig. 3 Unstable nominal motion: trajectory spirals to deformed equilibrium; Eq. (33) is not satisfied.

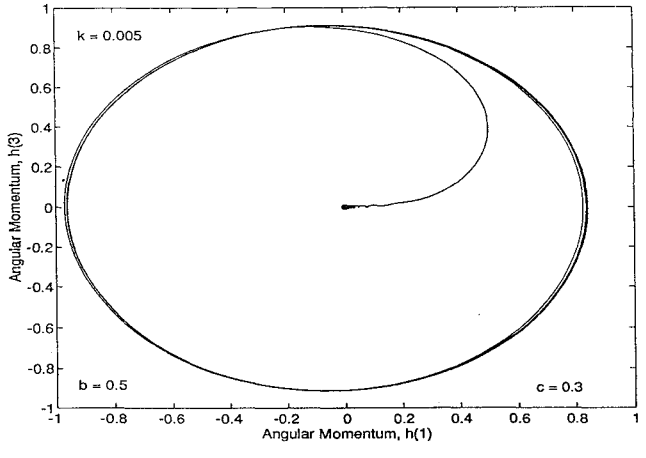

Fig. 4 Unstable nominal motion: trajectory spirals out to an apparent limit cycle; Eq. (33) is not satisfied.

approaches a different stable equilibrium, with nonzero limiting values of h_1 and x. This motion corresponds to a steady spin about a new major axis. In the third case (Fig. 4) the solution tends to a closed periodic orbit, which appears to be a limit cycle. This solution raises additional questions: Do limit cycles exist? If so, what parameters and/or initial conditions give rise to limit cycles?

We remark that the unsteady motions found by Levi[7] for a similar model are essentially limit cycles. Also dual-spin satellites exhibit limit cycle behavior for nonlinear damping[14] and nonlinear restoring force.[15] Thus, it would not be too surprising to find limit cycles in the present problem. In the following section we use numerical bifurcation results to argue that the apparent limit cycle is actually a transient motion and eventually settles down to a steady spin about a major axis of a deformed system.

Numerical Bifurcation Results

To determine whether Fig. 4 is actually a limit cycle, a bifurcation analysis is performed.[11] In this section we obtain bifurcation diagrams numerically, using the AUTO[10] continuation program. In addition to the pitchfork bifurcation described by Eq. (33), we find branches of limit points, a transcritical bifurcation, and a degenerate pitchfork corresponding to a transition from subcritical to supercritical behavior. In the following section we obtain an analytical expression for this degeneracy.

The bifurcation analysis is based on setting Eqs. (23–25) equal to zero and finding solutions to the resulting algebraic equations. It is straightforward to show that there are two isolated branches of equilibria satisfying $h_1 = h_2 = 0, h_3 = \pm 1$ and that these are unstable if Eq. (31) is satisfied. We do not consider these branches further, and we use the fact that all other equilibrium solutions satisfy $h_3 = p_n = 0$ to reduce the equilibrium equations to the following three equations for h_1, h_2, and x:

$$\varepsilon b\left[\left(h_1^2 - h_2^2\right)x + \varepsilon' h_1 h_2 x^2\right] + (I_1 - 1)h_1 h_2 = 0 \tag{34}$$

$$\varepsilon[(\varepsilon' - \varepsilon b)h_1 x - I_1 h_2](h_1 + \varepsilon b h_2 x) - kx D_1^2 = 0 \tag{35}$$

$$1 - h_1^2 - h_2^2 = 0 \tag{36}$$

where D_1 is defined as in Eq. (28). Note that these equations are independent of I_3.

The trivial solution branch is $h_2 = \pm 1, h_1 = x = 0$, and is the nominal solution for the spinning body. The stability of this branch is governed by Eq. (33). We are interested in the bifurcation which occurs for this relationship between the system parameters. We use AUTO[10] to trace branches of equilibria for constant values of k, while continuing in b. Figures 5–7 illustrate the three generic types of bifurcation diagrams that exist for this problem. These plots are for $\varepsilon = 0.1$, and plot the equilibrium value of h_1 vs b for different values of k. Following convention, solid curves represent branches of stable equilibria and dashed curves denote unstable branches. Note that Eqs. (34–36) are invariant under the transformation $(h_1, h_2, x) \mapsto (h_1, -h_2, -x)$; thus we identify two branches of equilibria with each branch of h_1 shown.

The three different types of bifurcation diagrams correspond to different ranges of k. For small k (Fig. 5), the pitchfork is subcritical; i.e., it opens to the left, and the bifurcating branches are unstable. There are also two isolated branches of stable equilibria that can not be found by continuation in b from the trivial solution. These branches are found by continuation in k from the trivial solution with a fixed value of b. The interesting thing here is that for any parameter values there are stable equilibria in addition to the trivial solution.

For an intermediate range of k (Fig. 6), the isolated branches connect with the pitchfork branches in a limit point. There are also additional isolated branches with limit points. These also cannot be

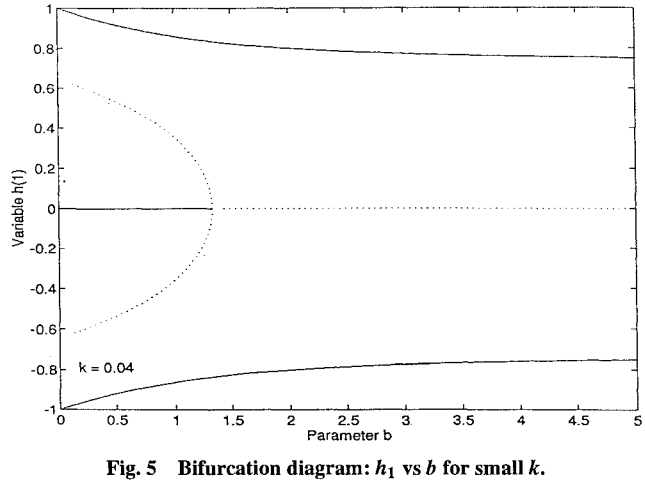

Fig. 5 Bifurcation diagram: h_1 vs b for small k.

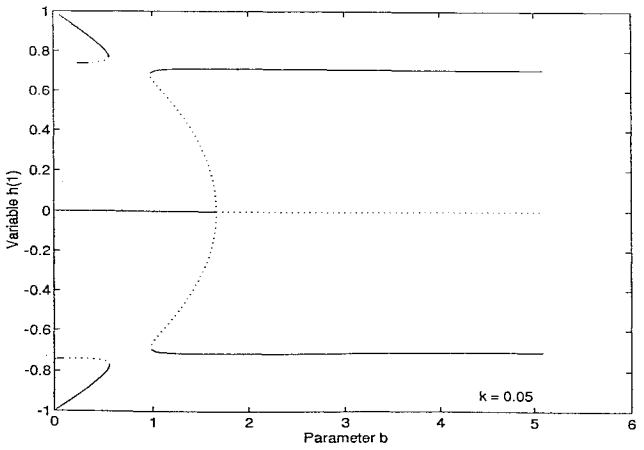

Fig. 6 Bifurcation diagram: h_1 vs b for intermediate k.

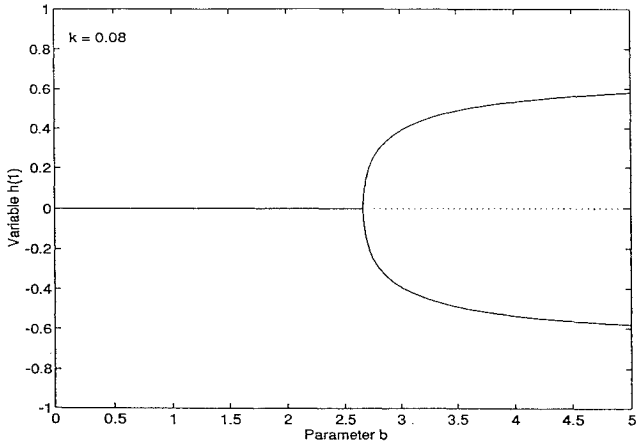

Fig. 7 Bifurcation diagram: h_1 vs b for large k.

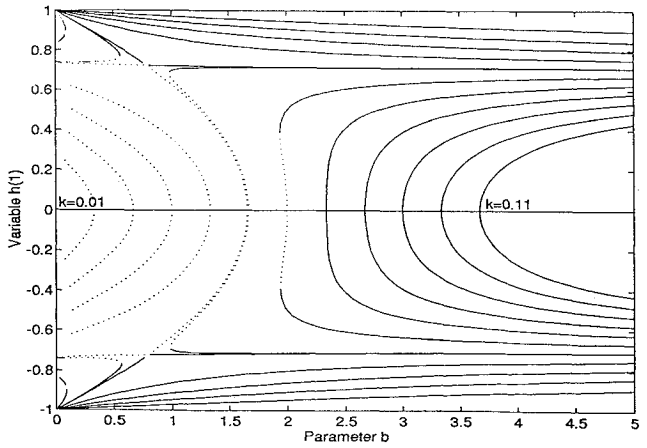

Fig. 8 Bifurcation diagram: h_1 vs b for a range of k.

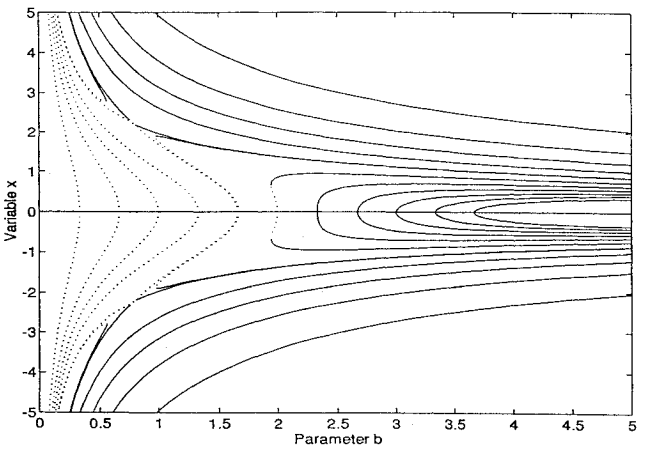

Fig. 9 Bifurcation diagram: x vs b for a range of k.

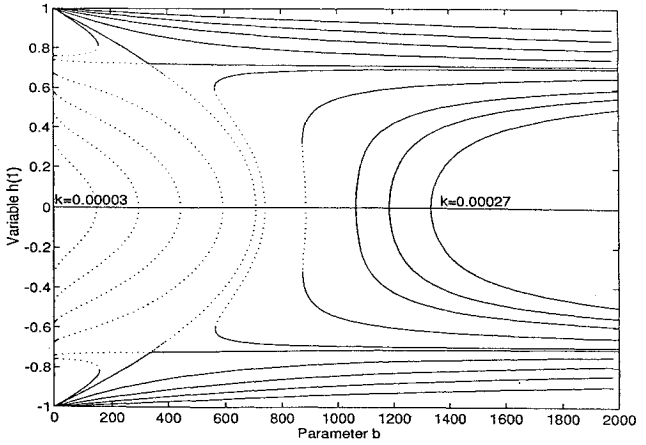

Fig. 10 Bifurcation diagram: h_1 vs b for a range of k; $\varepsilon = 0.00026$.

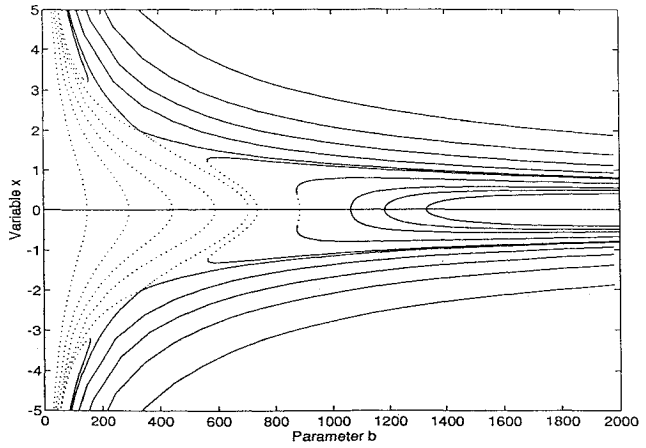

Fig. 11 Bifurcation diagram: x vs b for a range of k; $\varepsilon = 0.00026$.

found by continuation in b from the trivial solution, but rather are found by two-parameter continuation of the connected limit points. For this range of k, there is a range of b where the trivial solution is the only stable equilibrium, and two ranges of b where the trivial solution coexists with two other stable branches of equilibria. There is a critical value of k corresponding to the point where the connected limit points coalesce with the isolated limit points, giving rise to a transcritical bifurcation that can be seen in Figs. 8 and 9.

For large values of k (Fig. 7), the pitchfork is supercritical; i.e., it opens to the right, and the bifurcating branches are stable. For this range of k, the trivial solution, when, stable, is the only stable equilibrium (except for very small b). There is a critical value of k corresponding to the point where the subcritical pitchforks in Figs. 5 and 6 transition to supercritical pitchforks as in Fig. 7.

Figures 8 and 9 are composite bifurcation diagrams for a range of k. Figure 8 plots h_1 vs b, and Fig. 9 shows the value of x vs b. The mass fraction is $\varepsilon = 0.1$ in both figures. Since this value of ε is very large for ordinary precession damper applications, we also show bifurcation diagrams using a more realistic value, $\varepsilon = 0.00026$, based on the data in Ref. 5. Bifurcation diagrams for this value are shown in Figs. 10 and 11. Note that these plots are qualitatively similar to those in Figs. 8 and 9 but have much larger values of b.

The reason for constructing these bifurcation diagrams is to try to determine whether the apparent limit cycle in Fig. 4 is, in fact, a limit cycle. As Figs. 5 and 8 show, for given small k, there are two branches of stable equilibria (actually four, since each h_1 branch corresponds to two branches) with $h_1 \approx 1$. It is this equilibrium that the limit cycle is tending to as $t \to \infty$, as can be checked by careful

long-time integration of the differential equations. The two interesting values of k are those that correspond to the transcritical bifurcation and the degenerate pitchfork bifurcation. In the next section, we use Lyapunov–Schmidt reduction to obtain the analytical conditions for the occurrence of the degenerate pitchfork. There does not appear to be a straightforward way to obtain a similar result for the transcritical bifurcation.

Analytical Bifurcation Results

In this section we give the results of applying the Lyapunov–Schmidt reduction[12,13] to Eqs. (34–36) to obtain the conditions for the bifurcation from subcritical to supercritical pitchforks identified in the numerical studies of the preceding section. The details of the calculations are outlined in the Appendix.

We denote the vector equations (34–36) by

$$\boldsymbol{f}(\boldsymbol{y}, \lambda) = \boldsymbol{0} \tag{37}$$

with $\boldsymbol{y} = (h_1, h_2 - 1, x)$, and $\lambda = b - \beta$. The translations are introduced so that $\boldsymbol{f} = (\boldsymbol{0}, 0) = \boldsymbol{0}$ is a bifurcation point when k takes the bifurcation value $k = \varepsilon^2 b/(1 - I_1)$, given by Eq. (33).

At ordinary points where $\boldsymbol{f}(\boldsymbol{y}, \lambda) = \boldsymbol{0}$, the implicit function theorem provides the algorithm for tracing equilibrium branches $\boldsymbol{y}(\lambda)$ that form the main parts of the bifurcation diagrams of the preceding section. Because $(\boldsymbol{0}, 0)$ is a bifurcation point, the Jacobian of $\boldsymbol{f}$ at this point, denoted by $\mathrm{d}\boldsymbol{f}_{(\boldsymbol{0},0)}$, is singular, and the implicit function theorem is not applicable. Bifurcation theory[10–13] provides the necessary tools for tracing the bifurcating branches of equilibria. This theory is especially well developed for the scalar case where

$$\boldsymbol{f}(\boldsymbol{y}, \lambda) = \boldsymbol{0} \rightarrow g(u, \lambda) = 0 \tag{38}$$

with g a scalar function of a scalar variable u. The Lyapunov–Schmidt technique provides the algorithm for reducing $\boldsymbol{f}(\boldsymbol{y}, \lambda)$ to the scalar function $g(u, \lambda)$, where u is the component of $\boldsymbol{y}$ in the direction of the null space of $\mathrm{d}\boldsymbol{f}_{(\boldsymbol{0},0)}$.

Once the reduction is accomplished, well-known methods for the scalar problem may be applied. For example, a normal form for the pitchfork bifurcation is

$$g(u, \lambda) = \lambda u - u^3 = 0 \tag{39}$$

which is characterized by the value of g and its derivatives at (0, 0),

$$g = g_u = g_{uu} = g_\lambda = 0, \qquad g_{uuu} < 0, \qquad g_{u\lambda} > 0 \tag{40}$$

Any function $g(u, \lambda)$ that satisfies these conditions exhibits a supercritical pitchfork at (0, 0), as in Fig. 7. Alternatively, the function $g(u, \lambda) = \lambda u + u^3$ exhibits a subcritical pitchfork at the origin, as in Figs. 5 and 6. It is easy to see that the only difference in the given conditions is that $g_{uuu} > 0$ for the subcritical pitchfork. In the present problem, we are interested in determining conditions on the parameters for whether the bifurcation is subcritical or supercritical. This amounts to finding where g_{uuu} or $g_{u\lambda}$ changes sign. Thus, we do not require $g(u, \lambda)$ explicitly; we only need to check the conditions on its derivatives, as given by Eq. (40).

We find the derivatives by applying Lyapunov–Schmidt reduction, the details of which are discussed in the Appendix. We check that $g = g_u = g_{uu} = g_\lambda = 0$ are all satisfied, and we obtain the following remarkably simple expressions for the higher derivatives:

$$g_{u\lambda} = \varepsilon^2 I_1^2/(1 - I_1) \tag{41}$$

$$g_{uuu} = \frac{12\varepsilon^3 b^2 I_1^2[\varepsilon'(1 - I_1) + \varepsilon b(I_1 - 2)]}{(1 - I_1)^3} \tag{42}$$

Since $g_{u\lambda} > 0$ is independent of b, the test for subcritical vs supercritical depends on the sign of g_{uuu}, which simplifies to

$$\varepsilon'(1 - I_1) + \varepsilon b(I_1 - 2) \begin{cases} <0 & \Rightarrow \text{ supercritical} \\ =0 & \Rightarrow \text{ degenerate} \\ >0 & \Rightarrow \text{ subcritical} \end{cases} \tag{43}$$

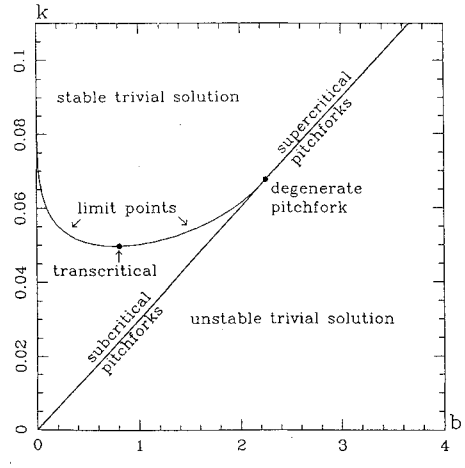

Fig. 12 Bifurcations in the bk plane; $I_1 = 0.6664$ and $\varepsilon = 0.1$.

Considering ε and I_1 as given, the critical value of b where the transition occurs is

$$b_{cr} = \varepsilon'(1 - I_1)/[\varepsilon(2 - I_1)] \tag{44}$$

The critical value of the spring constant is then obtained using Eq. (33),

$$k_{cr} = \varepsilon\varepsilon'/(2 - I_1) \tag{45}$$

Thus, if $k > k_{cr}$, then the bifurcation diagram is of the type shown in Fig. 7; otherwise, Fig. 5 or 6 is applicable. This leads to a design criterion for k and b: $k > k_{cr}$ ensures against the jump phenomenon, and b satisfying Eq. (33) ensures a stable trivial solution. The limit on b probably will not be restrictive in most designs, since b will necessarily be limited by placement inside the spacecraft. The complete picture is given by Fig. 12, which shows the bifurcation values of b and k. This figure is qualitatively unchanged by varying ε and I_1.

Conclusions

The motion of a torque-free rigid body with a precession damper has been characterized using a combination of numerical integration, numerical continuation, and analytical bifurcation techniques. Apparent limit cycles have been identified as transient motions. A transcritical bifurcation and subcritical and supercritical pitchforks have been located using bifurcation diagrams involving two parameters. The transition from subcritical to supercritical pitchfork bifurcation has been identified analytically using Lyapunov–Schmidt reduction.

Appendix: Details of the Lyapunov–Schmidt Reduction

Here we outline the calculations used to obtain the formula for the critical value of k, Eq. (45), following Golubitsky and Schaeffer.[12] The extensive algebra was performed using Mathematica.[16]

Several matrices and vectors are needed for the calculation. The Jacobian of $\boldsymbol{f}$ at the bifurcation point is

$$\mathrm{d}\boldsymbol{f}_{(\boldsymbol{0},0)} \triangleq \boldsymbol{D} = \begin{bmatrix} I_1 - 1 & 0 & -\varepsilon b \\ -\varepsilon I_1 & 0 & \varepsilon^2 b I_1/(I_1 - 1) \\ 0 & -2 & 0 \end{bmatrix} \tag{A1}$$

The null space of $\boldsymbol{D}$, that is, $\mathcal{N}(\boldsymbol{D})$, is spanned by the vector

$$\boldsymbol{n}_D = [\varepsilon b/(I_1 - 1), 0, 1] \tag{A2}$$

The range of $\boldsymbol{D}$, that is, $\mathcal{R}(\boldsymbol{D})$, is spanned by the two vectors

$$\boldsymbol{r}_1 = [1, \varepsilon I_1/(1 - I_1), 0] \tag{A3}$$

$$\boldsymbol{r}_2 = (0, 0, 1) \tag{A4}$$

The projection onto $\mathcal{R}(\boldsymbol{D})$ is

$$\boldsymbol{E} = \frac{1}{D_4}\begin{bmatrix} (I_1-1)^2 & \varepsilon I_1(1-I_1) & 0 \\ \varepsilon I_1(1-I_1) & \varepsilon^2 I_1^2 & 0 \\ 0 & 0 & D_4 \end{bmatrix} \tag{A5}$$

where

$$D_4 = (1-I_1)^2 + \varepsilon^2 I_1^2 \tag{A6}$$

We require additional derivatives of $\boldsymbol{f}(\boldsymbol{y}, \lambda)$, namely, $\mathrm{d}^2\boldsymbol{f}$, $\mathrm{d}^3\boldsymbol{f}$, $\boldsymbol{f}_\lambda$, and $\mathrm{d}\boldsymbol{f}_\lambda$, all of which are evaluated at $(\boldsymbol{0}, 0)$. We do not reproduce all of these results here, as they are easily computed. Note that $\mathrm{d}^2\boldsymbol{f}$ and $\mathrm{d}^3\boldsymbol{f}$ are third- and fourth-rank tensors, respectively.

We use two decompositions of $\mathbb{R}^3$,

$$\mathbb{R}^3 = \mathcal{N}(\boldsymbol{D}) \oplus M \tag{A7}$$

$$\mathbb{R}^3 = \mathcal{R}(\boldsymbol{D}) \oplus N \tag{A8}$$

where M is spanned by

$$\boldsymbol{m}_1 = (0, 1, 0) \tag{A9}$$

$$\boldsymbol{m}_2 = [1, 0, \varepsilon b/(1-I_1)] \tag{A10}$$

where N is spanned by

$$\boldsymbol{n}_R = [\varepsilon I_1/(I_1-1), 1, 0] \tag{A11}$$

Note that M and N are not unique and that we have chosen their bases so that the $\boldsymbol{m}_i$ are orthogonal to $\mathcal{N}(\boldsymbol{D})$, and $\boldsymbol{n}_R$ is orthogonal to $\mathcal{R}(\boldsymbol{D})$.

Although $\boldsymbol{D}$ is singular, it is a nonsingular transformation from M to $\mathcal{R}(\boldsymbol{D})$. We denote the inverse of this transformation by $\boldsymbol{D}^{-1}$ given by

$$\boldsymbol{D}^{-1} = \frac{1}{D_5}\begin{bmatrix} (I_1-1)^3 & -\varepsilon I_1(I_1-1)^2 & 0 \\ 0 & 0 & -D_5/2 \\ -\varepsilon b(I_1-1)^2 & \varepsilon^2 b I_1(I_1-1) & 0 \end{bmatrix} \tag{A12}$$

where

$$D_5 = \left[(1-I_1)^2 + \varepsilon^2 b^2\right]\left[(1-I_1)^2 + \varepsilon^2 I_1^2\right] \tag{A13}$$

The necessary formulas for the higher derivatives of g are then

$$g_{u\lambda} = \left\langle \boldsymbol{n}_R,\ \mathrm{d}\boldsymbol{f}_\lambda \boldsymbol{n}_D - \mathrm{d}^2\boldsymbol{f}\left(\boldsymbol{n}_D, \boldsymbol{D}^{-1}\boldsymbol{E}\boldsymbol{f}_\lambda\right)\right\rangle \tag{A14}$$

$$g_{uuu} = \left\langle \boldsymbol{n}_R,\ \mathrm{d}^3\boldsymbol{f}(\boldsymbol{n}_D, \boldsymbol{n}_D, \boldsymbol{n}_D) - 3\,\mathrm{d}^2\boldsymbol{f}\left(\boldsymbol{n}_D, \boldsymbol{D}^{-1}\boldsymbol{E}\,\mathrm{d}^2\boldsymbol{f}(\boldsymbol{n}_D, \boldsymbol{n}_D)\right)\right\rangle \tag{A15}$$

These are the expressions used to compute the derivatives in Eqs. (41) and (42).

Acknowledgment

We are grateful to Jeffrey Beck for many useful discussions on using AUTO.

References

[1]Hughes, P. C., *Spacecraft Attitude Dynamics*, Wiley, New York, 1986, Chaps. 3 and 4.

[2]Cloutier, G. J., "Nutation Damper Instability on Spin-Stabilized Spacecraft," *AIAA Journal*, Vol. 7, No. 11, 1969, pp. 2110–2115.

[3]Schneider, C. C., Jr., and Likins, P. W., "Nutation Dampers vs Precession Dampers for Asymmetric Spinning Spacecraft," *Journal of Spacecraft and Rockets*, Vol. 10, No. 3, 1973, pp. 218–222.

[4]Sarychev, V. A., and Sazonov, V. V., "Spin-Stabilized Satellites," *Journal of the Astronautical Sciences*, Vol. 24, No. 4, 1976, pp. 291–310.

[5]Cochran, J. E., Jr., and Thompson, J. A., "Nutation Dampers vs Precession Dampers for Asymmetric Spacecraft," *Journal of Guidance and Control*, Vol. 3, No. 1, 1980, pp. 22–28.

[6]Month, L. A., and Rand, R. H., "Stability of a Rigid Body with an Oscillating Particle: An Application of MACSYMA," *Journal of Applied Mechanics*, Vol. 52, No. 3, 1985, pp. 686–692.

[7]Levi, M., "Morse Theory for a Model Space Structure," *Dynamics and Control of Multibody Systems, Contemporary Mathematics*, Vol. 97, American Mathematical Society, Providence, RI, 1989, pp. 209–216.

[8]Kane, T. R., and Levinson, D. A., "A Passive Method for Eliminating Coning of Force-Free, Axisymmetric Rigid Bodies," *Journal of the Astronautical Sciences*, Vol. 40, No. 4, 1992, pp. 439–448.

[9]Chinnery, A. E., "Numerical Analysis of a Rigid Body with an Attached Spring-Mass-Damper," M.S. Thesis, Graduate School of Engineering, Air Force Inst. of Technology, Wright–Patterson AFB, OH, Dec. 1994.

[10]Doedel, E., "AUTO: Software for Continuation and Bifurcation Problems in Ordinary Differential Equations," California Inst. of Technology, Pasadena, CA, May 1986.

[11]Seydel, R., *From Equilbrium to Chaos: Practical Bifurcation and Stability Analysis*, Elsevier, New York, 1988, Chaps. 1–5.

[12]Golubitsky, M., and Schaeffer, D. G., *Singularities and Groups in Bifurcation Theory*, Vol. I, Springer–Verlag, New York, 1985, Chaps. 1 and 7.

[13]Rand, R. H., and Armbruster, D., *Perturbation Methods, Bifurcation Theory, and Computer Algebra*, Springer–Verlag, New York, 1987, Chap. 7.

[14]Likins, P. W., Tseng, G.-T., and Mingori, D. L., "Stable Limit Cycles due to Nonlinear Damping in Dual-Spin Spacecraft," *Journal of Spacecraft and Rockets*, Vol. 8, No. 6, 1971, pp. 568–574.

[15]Mingori, D. L., Tseng, G.-T., and Likins, P. W., "Constant and Variable Amplitude Limit Cycles in Dual-Spin Spacecraft," *Journal of Spacecraft and Rockets*, Vol. 9, No. 11, 1972, pp. 825–830.

[16]Wolfram, S., *Mathematica: A System for Doing Mathematics by Computer*, 2nd ed., Addison–Wesley, Redwood City, CA, 1991, Chap. 3.